Hindawi
International Journal of RF and Microwave Computer-Aided Engineering
Volume 2024, Article ID 9298815, 8 pages
https://doi.org/10.1155/2024/9298815

Research Article

Realization of a Wide Stopband Filter Using the Weakest Electric Field Method and Electromagnetic Hybrid Coupling Method

Xiaohei Yan and Minjie Guo

School of Mathematics, Physics, and Electronic Information Engineering, Guangxi Minzu Normal University, Chongzuo 532200, China

Correspondence should be addressed to Xiaohei Yan; yanxiaohei@gxnun.edu.cn

Received 8 November 2023; Revised 13 December 2023; Accepted 29 December 2023; Published 24 January 2024

Academic Editor: Guoan Wang

To enhance filter performance in terms of stopband, we propose a wide-stopband substrate-integrated waveguide filter based on the rejection of higher-order modes. The filter establishes the inner and outer coupling windows at the mode's weakest electric field to achieve mode suppression. Simultaneously, we employ the electromagnetic hybrid coupling theory to analyze the electromagnetic distribution of the particular modes and determine the dimensions of the coupling circular apertures and slits based on the extracted coupling coefficients to attain suppression of the specific modes. The filter successfully suppresses all higher-order modes having resonant frequencies below that of the TE_{150} mode, as demonstrated by simulation results. We conducted measurements and found that the filter has a center frequency of 4.78 GHz, a bandwidth of 100 MHz with a -3 dB attenuation, and a stopband of -25 dB that extends up to 16.62 GHz (i.e., 3.48 times the center frequency). Simulation and measurement results demonstrate a good correlation. This method, compared to other SIW filters, is easy to design, has a wider stopband range, can be readily applied to practical microwave communication systems, and has potential applications.

1. Introduction

For microwave device design, substrate-integrated waveguide (SIW) is an optimal option because of its high-quality factor, small size, low loss, and low cost. It is extensively utilized in the design of different microwave gadgets, including filters, couplers, diplexers, and antennas [1–7]. Nevertheless, since SIW exhibits inherent multimode resonance characteristics, filters designed using it frequently fall short of providing an adequate stopband width. To solve this issue, researchers have suggested multiple approaches to broadening the stopband of SIW filters.

To enhance the stopband width of the filter, multiple methods have been explored by researchers. In a study mentioned in [8], distinct shapes of SIW cavities were utilized to mitigate harmonic coupling. While this promotes out-of-band rejection performance, it also elevates the complexity of the filter design. Literature [9] suggests using cascaded low-pass filters to widen the filter stopband, but this method results in increased circuit size and loss, which is not ideal for integrating with communication systems. Literature [10] proposes setting the external or internal coupling window at the weakest electric field of a particular mode, but it only suppresses the TE_{120} higher-order mode. Literature [11] utilized an open/short-filled step impedance resonator to achieve a dual-pass band filter, which possesses a wide stopband width. However, due to the microstrip filter limitations, this method results in increased insertion loss at higher frequency bands. Literature [12] suggests a method for implementing a bandstop filter via dual-radial substrate-integrated waveguide resonant cavities. However, the shape of the filter acquired through this technique is more specialized and challenging to integrate into communication systems. In literature [13], researchers discovered that by etching complementary split-ring resonators (CSRRs) inside the upper surface of a substrate-integrated waveguide, bandstop filters could be achieved. However, when this method is used to extend the stopband width of a bandpass filter, it results in significant insertion loss. In literature [14], the introduction of transmission zeros for

harmonic suppression leads to increased out-of-band suppression. However, limiting the number of transmission zeros also limits the expansion of resistance bandwidth. In literature [15], a method for achieving a wide stopband in a filter involves selecting a cavity of a specific size to separate the first harmonic passband from the main mode passband, as well as staggering the higher-order harmonic couplings. However, this approach is constrained by the need for a cavity with a unique aspect ratio, making it suitable only for a narrow range of scenarios. In previous research [16], a multilayer coupling structure was used to create a wide stopband filter, but the filter only achieved a stopband of twice the center frequency, which was clearly inadequate. Subsequent research [17] addressed mode orthogonality by introducing offset port coupling, which was shown to improve stopband range. Nevertheless, the stopband extension range remained limited.

In light of the aforementioned research background, existing filters struggle to attain a well-rounded balance between stopband range, out-of-band rejection level, circuit structure, and design methodology. Therefore, this paper proposes a two-layer structure for a wide-stopband SIW bandpass filter. First, we eliminate higher-order modes (TE_{120}/TE_{210}, TE_{220}, TE_{230}/TE_{320}, TE_{140}/TE_{410}, and TE_{240}/TE_{420}) by positioning the inner and outer coupling windows at the spot with the weakest electric field. Next, using the electromagnetic hybrid coupling theory, we study the electromagnetic distribution of particular modes (TE_{130}, TE_{310}, and TE_{330}) with coupling coefficients. We then design the dimensions of the coupling circular holes and slits rationally. When the levels of electric and magnetic coupling are balanced, the TE_{130}/TE_{310} and TE_{330} higher-order modes can be sufficiently suppressed, leading to enhanced filter performance in terms of wider stopband and increased rejection levels. Afterward, we conducted processing and testing of the filter. The experimental results demonstrate high consistency between simulated and measured results, thus confirming the feasibility of the proposed design method.

2. Structure of the Filter

This study employs a substrate-integrated waveguide cavity structure with a double layer, as illustrated in Figure 1. It consists of three metal layers and two dielectric layers. The material used in the dielectric layer is ZYF300CA-P, which has a relative permittivity of 3, a loss tangent of 0.0018, and a thickness of 0.762 mm. The rectangular-shaped substrate-integrated waveguide cavity comprises two resonant cavities in each layer, as shown in Figure 1, labeled 1, 2, 3, and 4. The upper layer features resonant cavities 1 and 4, whereas the lower layer includes resonant cavities 2 and 3. Each resonant cavity is rectangular and operates in TE_{110} mode. The energy coupling between cavities no. 1 and no. 2 and no. 3 and no. 4 is through circular holes and gaps etched in the middle metal layer. Between cavities no. 2 and no. 3 in the lower layer, energy coupling occurs through a window at the center of the common edge. The input and output ports are placed in the middle of the sidewalls in resonant cavities no. 1 and no. 4, respectively. Both

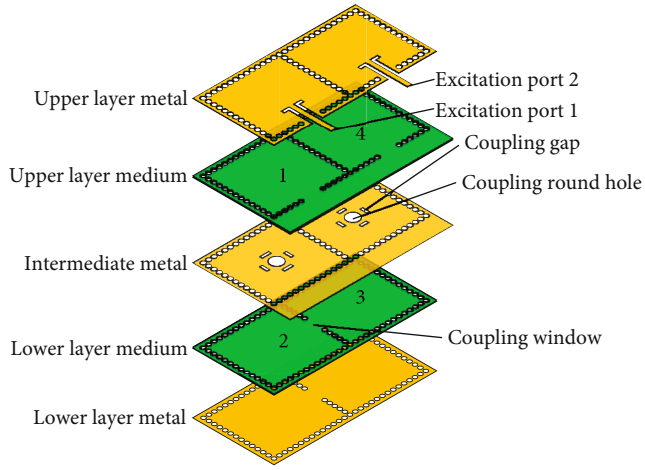

Figure 1: Structure of the filter.

of them utilize coplanar waveguides to facilitate the energy coupling between the source or load and the filter. The shape of the metal layer of the filter is shown in Figure 2. Following simulation optimization through the HFSS software, the filter's ultimate structural parameters are listed in Table 1.

3. Filter Design and Principle Analysis

3.1. SIW Resonant Cavity Theory. The SIW is a novel waveguide-like construct that exhibits electromagnetic field transmission characteristics similar to those of a rectangular waveguide. Nevertheless, the sidewalls of the SIW contain metallized through holes arranged in a periodically spaced pattern. This arrangement truncates the current that propagates along the longitudinal direction, generating a radiation effect. Thus, the transmission of the transverse magnetic wave TM_{mn0} mode is not possible in the SIW. In contrast, the transverse electric wave TE_{mn0} mode has solely a magnetic field component in the direction of longitudinal propagation, with no electric field component. Hence, the SIW rectangular resonant cavity can solely transmit TE_{mn0} modes, and the frequency equation for resonance is as follows:

$$f_{TEmn0} = \frac{c_0}{2\sqrt{\varepsilon_r}} \sqrt{\left(\frac{m}{W_{\text{eff}}}\right)^2 + \left(\frac{n}{L_{\text{eff}}}\right)^2}, \tag{1}$$

where c_0 is the speed of light in a vacuum, ε_r is the dielectric constant of the dielectric substrate, m and n are the number of modes along the width and length directions, respectively, and W_{eff} and L_{eff} are the equivalent width and length of the SIW structure, which are defined as follows:

$$\begin{aligned} W_{\text{eff}} &= W - \frac{d^2}{0.95p}, \\ L_{\text{eff}} &= L - \frac{d^2}{0.95p}, \end{aligned} \tag{2}$$

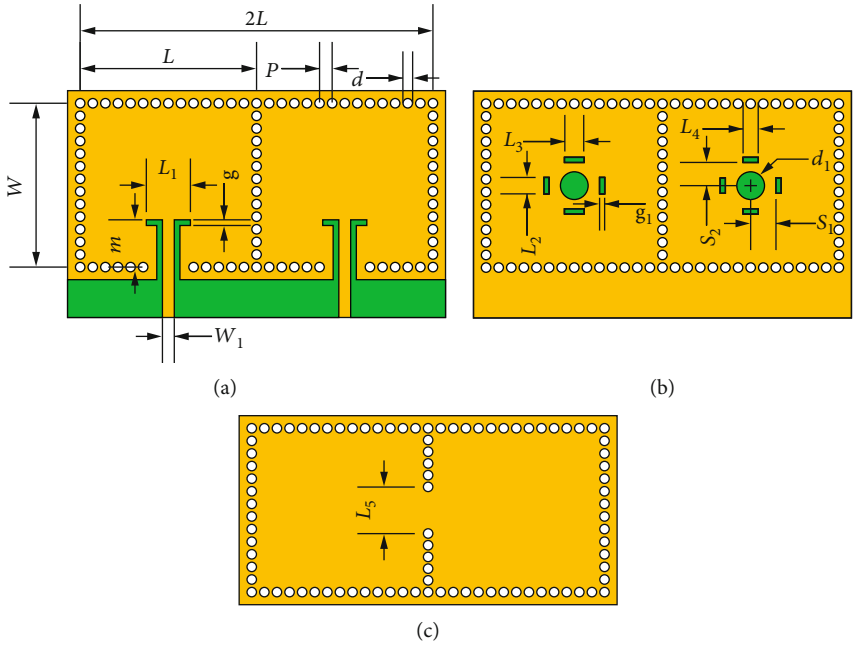

Figure 2: Dimensional drawings of the metal layers. (a) Upper metal layer. (b) Middle metal layer. (c) Lower metal layer.

Table 1: Structural parameters of the filter (unit: mm).

$L = 56$	$P = 2$	$d = 1.5$	$W = 26$
$m = 7.5$	$g = 0.9$	$L_1 = 7$	$W_1 = 1.88$
$L_2 = 2.6$	$L_3 = 3.1$	$g_1 = 0.8$	$L_4 = 2.4$
$d_1 = 4.4$	$S_1 = 4$	$S_2 = 3.68$	$L_5 = 7.4$

where the center distance between two rows of circular holes on the wide side of the cavity is denoted by W, the center distance between two columns of circular holes on the long side of the cavity is denoted by L, the diameter of the circular holes is denoted by d, and the circumcentric distance between adjacent circular holes is denoted by p.

In this design, the filter operates in the 5G n79 band. Therefore, the initial resonant frequency of the TE_{110} mode is assumed to be 4.75 GHz by setting $p = 2$ mm and $d = 1.5$ mm. The cavity dimensions can then be initially calculated following Eqs. (1) and (2).

$$\begin{aligned} W &= 26\text{mm}, \\ L &= 28\text{mm}. \end{aligned} \tag{3}$$

It is widely acknowledged that SIW resonant cavities possess an infinite number of resonant modes. In comparison to similar microwave filters, the harmonic passbands of the SIW are situated closer to the main mode passbands, which consequently restricts the stopband. To broaden the stopband range of the SIW filter, it is essential to suppress additional higher-order modes. The TE modes in the SIW rectangular resonant cavity occur in the following order as frequency increases: TE_{110}, TE_{120}/TE_{210}, TE_{220}, TE_{130}/TE_{310}, TE_{230}/TE_{320}, TE_{140}/TE_{410}, TE_{330}, TE_{240}/TE_{420}, and so forth. Table 2 displays their corresponding resonant frequencies. In order to achieve the wide stopband performance of the SIW filter, it is necessary to suppress the higher-order modes based on their resonant frequencies, from low to high.

Table 2: Resonant frequencies of partial modes of the rectangular resonant cavity.

Modes	F_0 (GHz)	Modes	F_0 (GHz)	Modes	F_0 (GHz)
TE_{110}	4.75	TE_{310}	10.96	TE_{410}	14.33
TE_{120}	7.34	TE_{230}	11.94	TE_{240}	14.67
TE_{210}	7.69	TE_{320}	12.31	TE_{420}	15.38
TE_{220}	9.51	TE_{140}	13.38	TE_{150}	16.52
TE_{130}	10.30	TE_{330}	14.27	TE_{430}	16.64

3.2. Analysis of Suppression Methods for Modes. The study employs a methodology of establishing external excitation ports and internal coupling windows at the weakest electric fields of specific modes in the SIW resonant cavity to fundamentally suppress the resonant coupling of higher-order modes. External excitation ports and internal coupling windows are located at the center of the sidewalls, i.e., at a and b in Figure 3. This design not only ensures the strongest magnetic coupling of the TE_{110} mode but also effectively suppresses other modes such as TE_{120}/TE_{210}, TE_{220}, TE_{230}/TE_{320}, TE_{140}/TE_{410}, and TE_{240}/TE_{420}. The input port is positioned at the center of the resonant cavity sidewalls, preventing the excitations of TE_{120}, TE_{220}, TE_{320}, TE_{140}, and TE_{240}/TE_{420} modes in the resonant cavity 1. The coupling window located at the sidewall's center suppresses

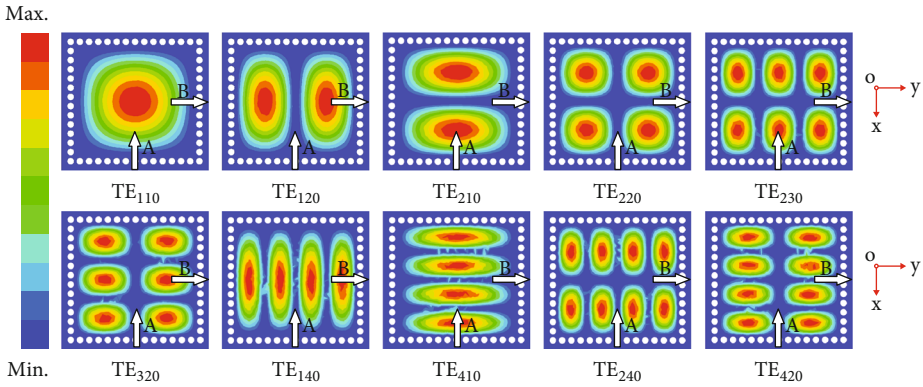

FIGURE 3: Electric field strength distribution of some modes in the SIW resonant cavity.

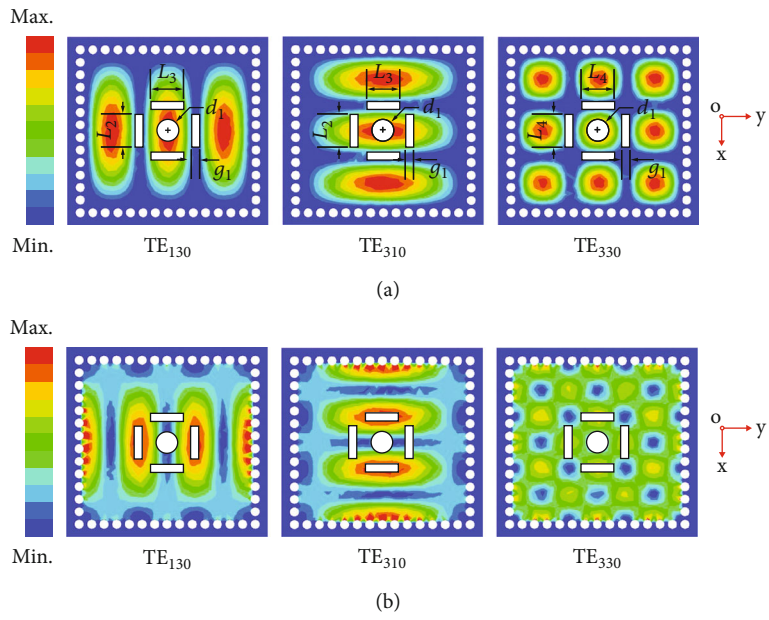

FIGURE 4: Position of the coupling structures in the electromagnetic field distribution of the corresponding modes of the resonant cavity. (a) Position of the coupling structures in the electric field distribution. (b) Position of the coupling structures in the magnetic field distribution.

the coupling of the TE_{210}, TE_{220}, TE_{230}, TE_{410}, and TE_{240}/TE_{420} modes between the resonant cavity 2 and the resonant cavity 3. However, electromagnetic hybrid coupling theory is necessary to suppress the coupling of the TE_{130}/TE_{310} and TE_{330} modes.

When only electrical or magnetic coupling exists between the two resonators, the coupling coefficient "k" can be determined by using the following equation:

$$k = \frac{f_2^2 - f_1^2}{f_2^2 + f_1^2}, \tag{4}$$

where f_1 and f_2 represent the odd-mode and even-mode resonant frequencies, respectively, that are generated when the two resonators are coupled. If there is both electric and magnetic coupling between two resonators, the total coefficient of coupling can be expressed through the following equation:

$$k_{\text{total}} = |k_m + k_e|, \tag{5}$$

where k_m is the magnetic coupling coefficient, which has a positive value, and k_e is the electric coupling coefficient, which has a negative value. Suppression of a mode can be achieved by introducing equal amounts of electric and magnetic coupling into the coupling of the two resonators so that the total coupling coefficient is approximately zero.

Based on the theory presented above, a coupling structure was designed in the SIW cavity (as shown in Figure 4) according to the electromagnetic field distribution of the TE_{130}/TE_{310} and TE_{330} modes. The coupling structure includes one coupling circular hole located at the center of the cavity and four coupling slits symmetrically distributed

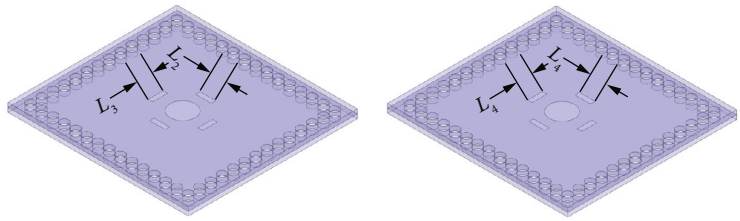

(a) (b)

FIGURE 5: Simulation models for extracting mode coupling coefficients. (a) TE_{130}/TE_{310} mode. (b) TE_{330} mode.

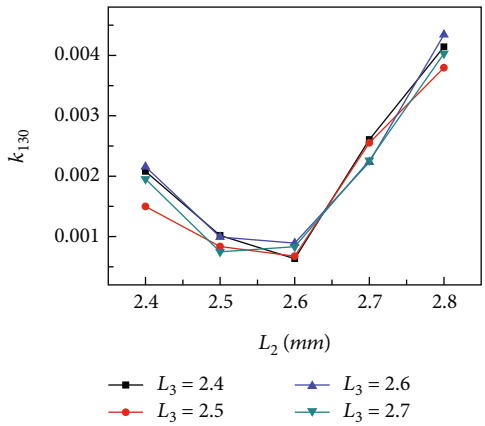

FIGURE 6: Curve of the coupling coefficient of TE_{130} mode as a function of L_2 and L_3.

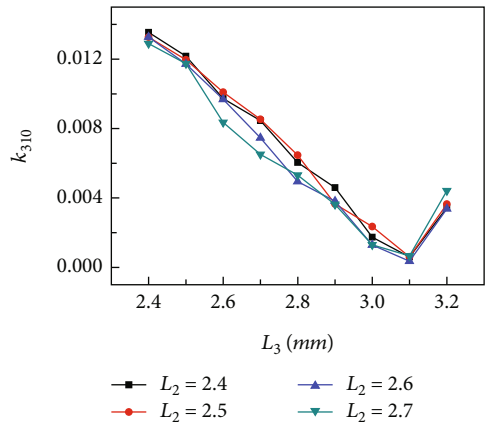

FIGURE 7: Curve of the coupling coefficient of TE_{310} mode as a function of L_3 and L_2.

in the center. The coupling circular hole has a diameter of d_1, and the coupling slits have a width of g_1. To achieve independent control over the degree of suppression of the TE_{130}, TE_{310}, and TE_{330} modes, distinct lengths are assigned to the coupling slits. Furthermore, the coupling structure between the resonant cavities of no. 1 and no. 2 is designed to suppress the TE_{130} and TE_{310} modes, while the coupling structure between resonant cavities no. 3 and no. 4 is intended to suppress the TE_{330} mode.

In the distribution of electromagnetic fields in a resonant cavity, the magnetic field is weaker in areas where the electric field is stronger and stronger in regions where the electric field is weaker. Using the TE_{130} mode as an illustration, the circular orifice with diameter d_1, along with the upper and lower pair of slits with length L_3, are strategically situated where the electric field is more potent to establish an electrical coupling. Conversely, the left and right pairs of slits with length L_2 are positioned where the electric field is weaker and the magnetic field is stronger to facilitate magnetic coupling. When appropriate values for d_1, L_2, and L_3 are selected, the electric and magnetic couplings can be balanced, resulting in a total coupling coefficient of 0 for the TE_{130} mode and effectively suppressing it. This approach can also be extended to suppress the TE_{310} and TE_{330} modes.

Based on the electric field distribution of the TE_{130}, TE_{310}, and TE_{330} modes, a simulation model was created using HFSS software to obtain the mode coupling coefficients, as depicted in Figure 5. The simulation model was

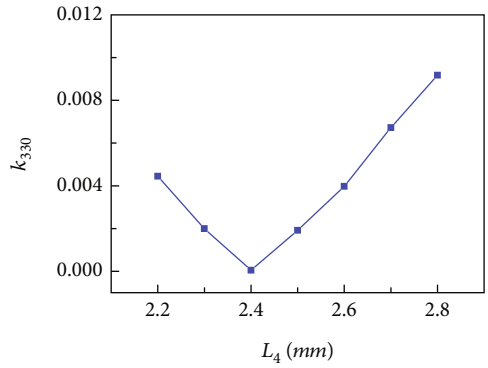

FIGURE 8: Curve of the coupling coefficient of TE_{330} mode as a function of L_4.

used to extract the coupling coefficients for the TE_{130}, TE_{310}, and TE_{330} modes, thereby confirming the feasibility of the electromagnetic hybrid coupling method. To ensure the optimal transmission performance of the primary TE_{110} mode within the passband, d_1 was set to 4.4 mm. Figure 6 depicts the influence curves resulting from changes in L_2 and L_3 on the coupling coefficients of TE_{130} modes extracted through simulation. The data suggests that k_{130}, the coupling coefficient of the TE_{130} modes, is primarily influenced by changes in L_2, with a comparatively smaller impact by changes in L_3. This is due to the fact that the

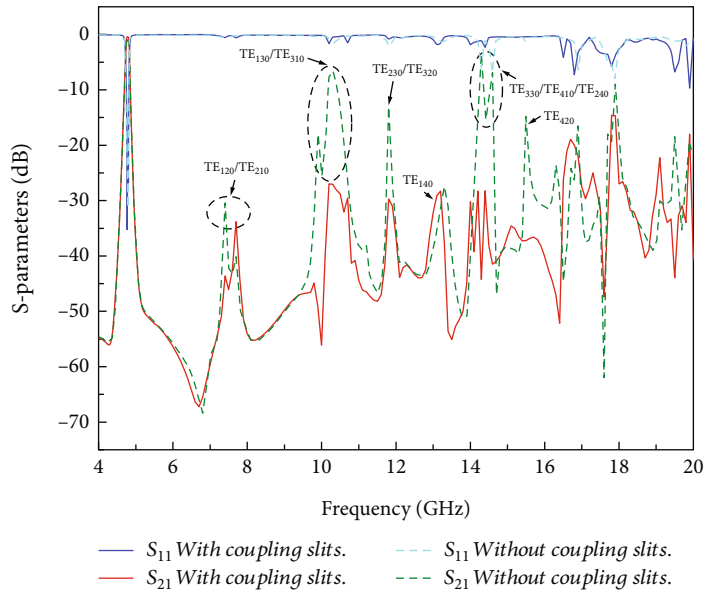

Figure 9: S-parameters of filters with and without coupling slits.

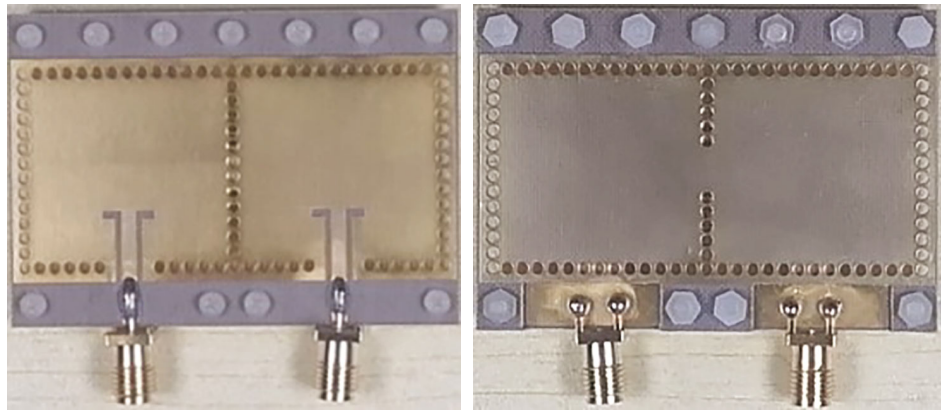

Figure 10: Filter object.

electric coupling of the TE_{130} mode is mainly provided by the circular hole located in the center of the cavity (the strongest electric field), and the electric field strength at the gap of length L_3 is much smaller compared to that at the circular hole, so the influence of the change of L_3 on the coupling coefficient is relatively small, while the magnetic field at the gap of length L_2 is the strongest, and the change of which results in a larger change of the magnetic coupling. When L_2 is set at 2.6 mm, the electric and magnetic couplings become nearly equal, resulting in a minimum value for the total coupling coefficient (k_{130}). Figure 7 shows the influence curve of L_2 and L_3 on the coupling coefficient of TE_{310} mode. It can be seen that the coupling coefficient (k_{310}) of TE_{310} mode is mainly affected by the change of L_3 , and the change of L_2 has a smaller influence on it for the same reason as mentioned above. The k_{310} reaches its minimum value when $L_3 = 3.1$ mm. Figure 8 displays the impact of the variation in L_4 on the coupling coefficient of TE_{330} mode. It is evident that k_{330} attains its minimum value at $L_4 = 2.4$ mm.

The SIW filter design, utilizing the electromagnetic hybrid coupling suppression method, enables targeted mode suppression, resulting in a wider stopband for the filter. Additionally, the coupling level of the filter can be flexibly controlled, allowing for adjustable filter bandwidth.

4. Results and Discussion

Figure 9 illustrates a comparison between the filter S-parameters obtained through simulation by solely utilizing the electric coupling of round holes between the no. 1 and no. 2 resonance cavities and between the no. 3 and no. 4 resonance cavities and the S-parameters obtained via simulation employing the electromagnetic hybrid coupling method in this particular design. When using only the electric coupling of round holes, it is evident that the weakest electric field method is efficient in suppressing higher-order modes. The TE_{120}/TE_{210}, TE_{220}, and TE_{140} modes can be suppressed better by the weakest electric field method, while the TE_{230}/TE_{320}, TE_{410}, and TE_{240}/TE_{420}

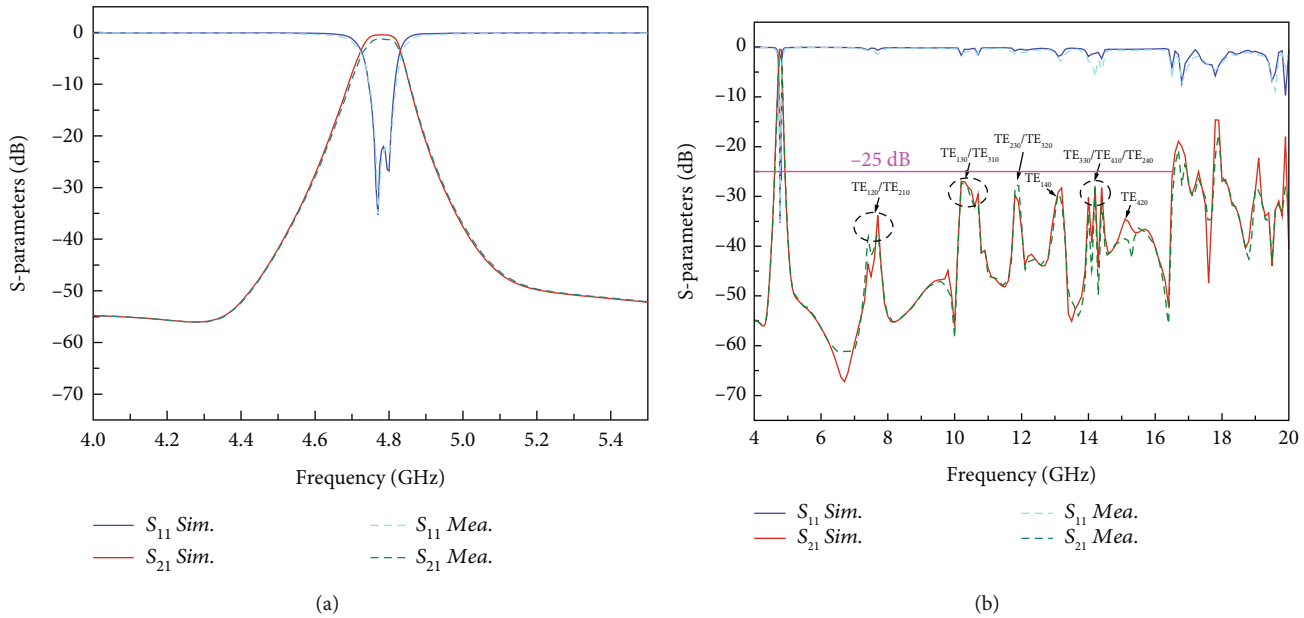

FIGURE 11: Simulated and measured filter S-parameters. (a) The passband transmission response of the filter. (b) The stopband transmission response of the filter.

modes are not sufficiently suppressed. The higher-order modes TE_{130}/TE_{310} and TE_{330} exhibit a stronger output currently, as they cannot be suppressed by the weakest electric field method. However, using the electromagnetic hybrid coupling method improves the suppression of not only the TE_{130}/TE_{310} and TE_{330} higher-order modes but also the TE_{230}/TE_{320}, TE_{410}, and TE_{240}/TE_{420} higher-order modes. The preceding findings support the efficacy of the electromagnetic hybrid coupling technique for targeted suppression of higher-order modes and enhancement of the filter stopband width.

Based on the dimensions listed in Table 1, the physical filter was processed by the PCB process, and the two layers of SIW cavities were mounted by screws to press the gap between the upper and lower cavities to prevent the leakage of electromagnetic energy. The physical filter is shown in Figure 10. To conduct the physical examination, solder SMA-KHD coaxial connectors on the filter's input and output ports and connect them to an Agilent E8363C model network vector analyzer for measurement. Figure 11 displays the simulated and measured S-parameters of the filter. The measured and simulated S-parameter curves display overall consistency, revealing a center frequency of 4.78 GHz, a bandwidth of 100 MHz at -3 dB, and a stopband at -25 dB that can be extended up to 16.62 GHz (i.e., 3.48 times the center frequency). The simulation exhibits an insertion loss of approximately -0.47 dB in the passband, while the measured insertion loss is 0.8 dB lower than the simulated value. Processing error, dielectric loss, and conversion structure loss are the primary reasons for the discrepancy between the measured and modeled values.

Table 3 presents a comparison of our proposed filter's performance with the SIW filters in the references. The filter proposed in this paper shows significant advantages in terms of insertion loss and blocking bandwidth, and the design methodology used is simple and easy to implement. Additionally, the filter employs a cascade structure that results in a more compact design for seamless integration into the communication system.

TABLE 3: Comparison with similar filters in the literature.

Refs.	F_0 (GHz)	Relative bandwidth (%)	Filter order	Insertion loss (dB)	Resistance bandwidth
[14]	20	2.75	4	2.78	20 dB/1.90f_0
[15]	10	1.51	3	2.91	25 dB/2.10f_0
[16]	13	4.55	2	1.5	20 dB/2.39f_0
[17]	15	4	5	2.3	50 dB/1.96f_0
This work	4.78	2.1	4	1.26	25 dB/3.48f_0

5. Conclusions

To enhance the filter's stopband performance, this paper proposes a wide-stopband filter for substrate-integrated waveguides that rejects higher-order modes. The filter effectively suppresses the mode by placing the inner and outer coupling windows at the mode's weakest electric field. Meanwhile, the paper presents the applications of electromagnetic hybrid coupling theory in analyzing the electromagnetic distribution of specific modes and in designing the size of coupling circular holes and slots based on the extracted coupling coefficients to achieve specific mode suppression. The results demonstrate that the filter center frequency is 4.78 GHz, with a -3 dB bandwidth of 100 MHz and an extended -25 dB stopband of 16.62 GHz (i.e., 3.48 times the center frequency). All higher-order modes with

resonant frequencies below the TE_{150} mode's resonant frequency are effectively suppressed by the filter. Compared to other SIW filters, this approach features a simple design and a broader stopband range. It can be easily implemented in real-world microwave communication systems and has promising applications.

Data Availability

The data used to support the findings of this study are available from the corresponding author upon request.

Conflicts of Interest

The authors declare that there is no conflict of interest regarding the publication of this paper.

Acknowledgments

This work is supported by the Chongzuo Science and Technology Program Project (No. 2023ZC025654), the School-level Research Project of Guangxi Minzu Normal University (No. 2022SP007), the first batch of the 2021 Industry-University Cooperation Collaborative Education Project of the Department of Higher Education, Ministry of Education (No. 202101139002), the Basic Research Ability Improvement Project for Young and Middle-aged Teachers in Guangxi Universities (No. 2023KY0793), and the Guangxi Natural Science Foundation (No. 2022JJB150010).

References

[1] M. Bozzi, A. Georgiadis, and K. Wu, "Review of substrate-integrated waveguide circuits and antennas," *IET Microwaves, Antennas & Propagation*, vol. 5, no. 8, pp. 909–920, 2011.

[2] X.-P. Chen and K. Wu, "Substrate integrated waveguide filter: basic design rules and fundamental structure features," *IEEE Microwaves Magazine*, vol. 15, no. 5, pp. 108–116, 2014.

[3] A. Pourghorban Saghati, A. Pourghorban Saghati, and K. Entesari, "Ultra-miniature SIW cavity resonators and filters," *IEEE Transactions on Microwave Theory and Techniques*, vol. 63, no. 12, pp. 4329–4340, 2015.

[4] J. Schorer, J. Bornemann, and U. Rosenberg, "Mode-matching design of substrate mounted waveguide (SMW) components," *IEEE Transactions on Microwave Theory and Techniques*, vol. 64, no. 8, pp. 2401–2408, 2016.

[5] J. Li, W. X. Zhen, X. M. Wei, Y. J. Huang, and G. J. Wen, "Millimeter-wave substrate integrated waveguide bandpass filters based on stepped-impedanceE-shaped defected ground structures," *International Journal of RF and Microwave Computer-Aided Engineering*, vol. 32, no. 11, Article ID e23340, 2022.

[6] Y. C. Zhang, J. Q. Ge, and G. Wang, "Enabling electrically tunable radio frequency components with advanced microfabrication and thin film techniques," *Journal of Central South University*, vol. 29, no. 10, pp. 3248–3260, 2022.

[7] Y. M. Huang, W. Jiang, H. Y. Jin et al., "Substrate-integrated waveguide power combiner/divider incorporating absorbing material," *IEEE Microwave and Wireless Components Letters*, vol. 27, no. 10, pp. 885–887, 2017.

[8] K. Zhou, C. X. Zhou, and W. Wu, "Substrate integrated waveguide dual-band filter with wide-stopband performance," *Electronics Letters*, vol. 53, no. 16, pp. 1121–1123, 2017.

[9] T. S. Yun, H. Nam, J. Y. Kim et al., "Harmonics suppressed substrate-integrated waveguide filter with integration of low-pass filter," *Microwave and Optical Technology Letters*, vol. 50, no. 2, pp. 447–450, 2008.

[10] P. Chu, K. L. Zheng, F. Xu, and K. Wu, "Substrate integrated waveguide resonator with harmonic suppression," *Electronics Letters*, vol. 54, no. 24, pp. 1388-1389, 2018.

[11] W. Jiang, W. Shen, T. Wang, Y. M. Huang, Y. Peng, and G. Wang, "Compact dual-band filter using open/short stub loaded stepped impedance resonators (OSLSIRs/SSLSIRs)," *IEEE Microwave and Wireless Components Letters*, vol. 26, no. 9, pp. 672–674, 2016.

[12] M. N. Husain, G. S. Tan, and K. S. Tan, "Design of a substrate integrated waveguide bandstop filter using dual-radial cavity resonators," in *2014 IEEE REGION 10 SYMPOSIUM*, pp. 6–9, Kuala Lumpur, Malaysia, 2014.

[13] J.-A. Wang, D. Li, Y. Liu, Z. Chen, Z. Zheng, and Y. Deng, "Compact substrate integrated waveguide bandstop filter based on CSRRs," in *2020 IEEE Asia-Pacific microwave conference (APMC)*, pp. 222–224, Hong Kong, Hong Kong, 2020.

[14] F. Zhu, W. Hong, J. X. Chen, and K. Wu, "Wide stopband substrate integrated waveguide filter using corner cavities," *Electronics Letters*, vol. 49, no. 1, pp. 50–52, 2013.

[15] K. Zhou, C.-X. Zhou, and W. Wu, "Resonance characteristics of substrate-integrated rectangular cavity and their applications to dual-band and wide-stopband bandpass filters design," *IEEE Transactions on Microwave Theory and Techniques*, vol. 65, no. 5, pp. 1511–1524, 2017.

[16] D. H. Jia, Q. Y. Feng, Q. Y. Xiang, and K. Wu, "Multilayer substrate integrated waveguide (SIW) filters with higher-order mode suppression," *IEEE Microwave and Wireless Components Letters*, vol. 26, no. 9, pp. 678–680, 2016.

[17] P. Chu, L. Guo, L. Zhang, F. Xu, W. Hong, and K. Wu, "Wide stopband substrate integrated waveguide filter implemented by orthogonal ports' offset," *IEEE Transactions on Microwave Theory and Techniques*, vol. 68, no. 3, pp. 964–970, 2020.